

Suppression and Spatial Variation of Early Galaxies and Minihalos

Dmitriy Tseliakhovich^{1*}, Rennan Barkana² & Christopher M. Hirata³

¹ *California Institute of Technology, M/C 249-17, Pasadena, California 91125, USA*

² *Raymond and Beverly Sackler School of Physics and Astronomy, Tel Aviv University, Tel Aviv 69978, Israel*

³ *California Institute of Technology, M/C 350-17, Pasadena, California 91125, USA*

December 12, 2010

ABSTRACT

We study the effect of the relative velocity of dark matter and baryonic fluids after the epoch of recombination on the evolution of the first bound objects in the early universe. Recent work has shown that, although relative motion of the two fluids is formally a second order effect in density, it has a dramatic impact on the formation and distribution of the first cosmic structures. Focusing on the gas content, we analyze the effect of relative velocity on the properties of halos over a wide range of halo masses and redshifts. We calculate accurately the linear evolution of the baryon and dark matter fluctuations, and quantify the resulting effect on halos based on an analytical formalism that has been carefully checked with simulations in the case with no relative velocity. We estimate the effect on the abundance of and gas fraction in early halos. We find that the relative velocity effect causes several changes: (i) the characteristic mass that divides gas-rich and gas-poor halos is increased by roughly an order of magnitude, from $2 \times 10^4 M_\odot$ to about $2 \times 10^5 M_\odot$; (ii) this characteristic mass has a large scatter (full width at half maximum is $\sim 1.5 \times 10^5 M_\odot$ at $z = 20$); (iii) the fraction of baryons in star-less gas minihalos is suppressed by a factor of 4 at $z = 20$; (iv) the fraction of baryons in halos that can cool and form stars is suppressed by a factor of 1.5 at $z = 20$; and (v) there are enhanced spatial variations of these various fractions.

Key words: dark ages, reionization, first stars, large scale structure of the Universe.

1 INTRODUCTION

One of the most important questions in astrophysics today is understanding the formation and evolution of the first bound structures. Significant theoretical and observational efforts are devoted to understanding the properties of the first galaxies and minihalos, at what redshifts they form and how they influence the epoch of reionization. Observations, most notably of the cosmic microwave background (CMB), have established the basic parameters for the initial conditions for structure formation (Bennett et al. 2003), thus providing a foundation for theoretical work on the first structures. Advances in computation have made it possible to simulate the formation of the first stars (Abel, Bryan & Norman 2002; O’Shea et al. 2005; Yoshida et al. 2008). Meanwhile, several efforts are underway to probe the structure of the intergalactic medium (IGM) during the reionization epoch using the 21 cm line of hydrogen, and second-generation experiments may be able to explore the early stages of reionization.

To answer these and many other questions it is imperative to know the correct initial conditions that led to the formation of the first bound objects and to account for all subtle effects that influence evolution of the density perturbations after recombination. The critical role of initial conditions has been discussed by Naoz, Yoshida, & Barkana (2010), who showed that three commonly used setups lead to significantly different abundances and properties of the first star-forming gas clouds as well as first gas-rich minihalos.

There are two major classes of early-type objects that must be analyzed. The first class consists of large halos in which the gas can cool and form stars; these are the presumed sites of the first dwarf galaxies, which represent the first source of metals in the Universe, and provide ultraviolet photons that begin the decoupling of the hydrogen spin temperature from the CMB (Madau, Meiksin & Rees 1997) and eventually start the epoch of reionization. The second class consists of smaller halos (“minihalos”) that are too small for molecular cooling, but still affect the epoch of reionization by acting as a sink for ionizing photons (Haiman, Abel & Madau 2001; Barkana & Loeb 2002;

* E-mail: dimlyus@caltech.edu

Iliev, Scannapieco & Shapiro 2005; Ciardi et al. 2005) and may generate a 21 cm signal from collisional excitation of HI (e.g. Iliev et al. 2003; Furlanetto & Oh 2006). It is important to understand both the abundance and distribution of halos, as well as the precise boundaries separating halos that undergo cooling and star formation, those that collect baryons in their potential wells but do not cool, and the lightest halos that exist only as dark matter structures and do not collect gas.

An important effect that was previously overlooked is that of the relative velocity of dark matter and baryonic fluids (Tselikhovich & Hirata 2010). This effect leads to power suppression on scales that correspond to the first bound halos between $10^4 M_\odot$ and $10^8 M_\odot$ and delays the formation of the first objects. More importantly this effect introduces scale-dependent bias and stochasticity, leading to significant qualitative changes in the distribution of the first objects. The relative velocity effect is especially important on the small scales where the first stars and galaxies form. Introduction of this effect dramatically changes the gas distribution inside the first halos and changes the characteristic mass of gas-rich objects. Dalal, Pen & Seljak (2010) recently calculated analytically the effect on the gas content of halos and found a large effect on the fluctuations of the Lyman- α background at high redshifts. Their analysis, however, was based on a very simplified model of which halos can form stars and in what abundance. In this paper we carry out a detailed analytical study of the distribution of gas and stars in the first halos.

The rest of the paper is organized as follows. Section 2 reviews the relative velocity effect (Sec. 2.1) and improves the analysis of Tselikhovich & Hirata (2010) to account for spatial variation of the sound speed (Sec. 2.2). Section 3 then investigates the early halos and their gas content, focusing on computation of the filtering mass (Sec. 3.1) and then examining the fraction of baryons in minihalos and in larger halos that can cool, including an analysis of spatial variations in the baryon budget (Sec. 3.2 and 3.3). We summarize our results in Sec. 4 and compare them to other recent work.

The numerical results and plots shown in this paper assume a cosmology with present-day baryon density $\Omega_{b,0} = 0.044$, CDM density $\Omega_{c,0} = 0.226$, dark energy density $\Omega_{\Lambda,0} = 0.73$, Hubble constant $H_0 = 71 \text{ km s}^{-1} \text{ Mpc}^{-1}$, and adiabatic primordial perturbations of variance $\Delta_\zeta^2(k_*) = 2.42 \times 10^{-9}$ at $k_* = 0.002 \text{ Mpc}^{-1}$ and with slope $n_s = 0.96$.

2 INITIAL CONDITIONS FOR HALO FORMATION

In this section we detail the formalism necessary for generation of correct initial conditions taking into account two important effects that are often overlooked in the literature. First of all we introduce the effect of relative velocity of dark matter and baryonic fluids after recombination. This effect, first studied in Tselikhovich & Hirata (2010), is nominally a second order effect in the perturbation theory of density evolution and hence has been ignored in studies based on the linear theory. Secondly, we emphasize the importance of a correct treatment of the sound speed variations in the time between recombination and $z \sim 200$ due to residual Compton heating of the electrons on the CMB photons. As we

show later in the paper, both effects play a significant role during the epoch of first halo formation and dramatically impact gas fractions in the first bound objects.

2.1 Relative velocity of dark matter and baryonic fluids

Before recombination, the baryons are tightly coupled to the photons and the sound speed is highly relativistic, $\sim c/\sqrt{3}$. As the universe expands and cools the electrons recombine with the protons and the universe becomes transparent, leading to a kinematic decoupling of the baryons from the radiation around $z_{\text{dec}} \approx 1000$. After recombination the sound speed of the baryons drops precipitously down to thermal velocities, whereas the dark matter velocity remains unaffected, and after recombination the dark matter motion with respect to the baryons becomes supersonic. The relative velocity can be written as:

$$\mathbf{v}_{\text{bc}}(\mathbf{k}) = \frac{\hat{\mathbf{k}}}{ik} [\theta_{\text{b}}(\mathbf{k}) - \theta_{\text{c}}(\mathbf{k})], \quad (1)$$

where $\hat{\mathbf{k}}$ is a unit vector in the direction of \mathbf{k} , and $\theta \equiv a^{-1} \nabla \cdot \mathbf{v}$ is the velocity divergence (we use comoving coordinates).

The variance of this relative velocity is

$$\begin{aligned} \langle v_{\text{bc}}^2(\mathbf{x}) \rangle &= \int \frac{dk}{k} \Delta_\zeta^2(k) \left[\frac{\theta_{\text{b}}(k) - \theta_{\text{c}}(k)}{k} \right]^2 \\ &= \int \frac{dk}{k} \Delta_{\text{vbc}}^2(k), \end{aligned} \quad (2)$$

where $\Delta_\zeta^2(k) = 2.42 \times 10^{-9}$ is the initial curvature perturbation variance per $\ln k$. Integration of Eq. (2) at the time of recombination¹ ($z_{\text{rec}} = 1020$) shows that the dark matter moves relative to the baryons with root-mean square velocity $\sim 30 \text{ km s}^{-1}$ corresponding to a Mach number of $\mathcal{M} \equiv v_{\text{bc}}/c_s \sim 5$. This supersonic relative motion allows baryons to advect out of the dark matter potential wells and significantly suppresses the growth of structure at wave numbers higher than

$$k_{\text{vbc}} \equiv \frac{aH}{\langle v_{\text{bc}}^2 \rangle^{1/2}} \Big|_{\text{dec}} = \frac{k_{\text{J}}}{\mathcal{M}} \sim 40 \text{ Mpc}^{-1}, \quad (3)$$

where k_{J} is the Jeans wave number.

As shown in Tselikhovich & Hirata (2010) the relative velocity of the baryons and cold dark matter (CDM) is coherent over scales of several comoving Mpc and the velocity in each coherence region is well-described by a 3-dimensional Gaussian probability distribution with variance

$$\sigma_{\text{vbc}}^2 = \langle |\mathbf{v}_{\text{bc}}(\mathbf{x})|^2 \rangle. \quad (4)$$

(Note that this is the *total* variance, i.e., including velocities in all 3 directions; the variance per axis is smaller by a factor of 3.)

To see how the relative motion of baryons and dark matter affect the formation of the first objects we need to solve a system of evolution equations that incorporate this effect.

¹ Technically the effective redshift of kinematic decoupling (Eisenstein & Hu 1998), since recombination is an extended process.

The system of equations describing a high- k perturbation mode in the presence of a background relative velocity is

$$\begin{aligned}\frac{\partial \delta_c}{\partial t} &= \frac{i}{a} \mathbf{v}_{bc}^{(bg)} \cdot \mathbf{k} \delta_c - \theta_c, \\ \frac{\partial \theta_c}{\partial t} &= \frac{i}{a} \mathbf{v}_{bc}^{(bg)} \cdot \mathbf{k} \theta_c - \frac{3H^2}{2} (\Omega_c \delta_c + \Omega_b \delta_b) - 2H\theta_c, \\ \frac{\partial \delta_b}{\partial t} &= -\theta_b, \text{ and} \\ \frac{\partial \theta_b}{\partial t} &= -\frac{3H^2}{2} (\Omega_c \delta_c + \Omega_b \delta_b) - 2H\theta_b + \frac{c_s^2 k^2}{a^2} \delta_b.\end{aligned}\quad (5)$$

The v_{bc} terms are nominally second order in perturbation theory, and hence one may wonder why they, rather than other second-order terms, are included. The reason is that the expansion parameter for these terms is not the density perturbation δ , but rather the ratio of the advection terms (e.g. $v_{bc}^{(bg)} k \delta_c / a$ in the δ_c equation) to the linear terms (e.g. $\partial \delta_c / \partial t \sim \delta_c / H$). This ratio is

$$\frac{v_{bc}^{(bg)} k}{aH}.\quad (6)$$

One can see that this expansion parameter increases as one goes to smaller scales and is of order unity at $k \sim k_{vbc}$. Thus the v_{bc} terms become nonperturbative at small scales $k > k_{vbc}$, and when treating these small scales one must keep these terms even if they are formally higher order in the perturbation theory.

2.2 Complete heating model

The system of equations of Eq. (5) assumes a spatially uniform sound speed which is a good first-order approximation. However, as shown in Naoz & Barkana (2005), it underestimates baryon density fluctuations by more than 30 percent at $z = 100$ and 10 percent at $z = 20$ for large wavenumbers. A fully correct treatment of baryon density evolution requires analysis of the Compton heating from the CMB on the sound speed and fluctuations in the temperature distribution. Following Naoz & Barkana (2005), we re-write the sound speed term of the last equation of Eq. (5) as

$$\frac{c_s^2 k^2}{a^2} \delta_b \rightarrow \frac{k^2}{a^2} \frac{k_B \bar{T}}{c^2 \mu m_H} (\delta_b + \delta_T),\quad (7)$$

where δ_T is the temperature perturbation which evolves as:

$$\frac{d\delta_T}{dt} = \frac{2}{3} \frac{d\delta_b}{dt} + \frac{x_e(t)}{t_\gamma} a^{-4} \left\{ \delta_\gamma \left(\frac{\bar{T}_\gamma}{\bar{T}} - 1 \right) + \frac{\bar{T}_\gamma}{\bar{T}} (\delta_{T_\gamma} - \delta_T) \right\}.\quad (8)$$

The second term on the right-hand side accounts for the Compton scattering of the CMB photons on the residual electrons from recombination. Here $x_e(t)$ is the electron fraction relative to the total number density of gas particles², $\bar{T}_\gamma = [2.725 \text{ K}] / a$ is the mean CMB temperature, and

$$t_\gamma^{-1} \equiv \frac{8}{3} \rho_\gamma^0 \frac{\sigma_T c}{m_e} = 8.55 \times 10^{-13} \text{ yr}^{-1},\quad (9)$$

² This is different from the recombination literature, which often takes x_e to be normalized to the number of hydrogen nuclei. At low redshifts these differ by 8 per cent due to the presence of helium.

where σ_T is the Thomson scattering cross section, ρ_γ^0 is the photon energy density at $z = 0$, and \bar{T} is the average temperature of the baryons, which can be calculated using the first law of thermodynamics:

$$\frac{d\bar{T}}{dt} = -2H\bar{T} + \frac{x_e(t)}{t_\gamma} (\bar{T}_\gamma - \bar{T}) a^{-4}.\quad (10)$$

Accounting for Compton heating of the residual electrons by the CMB photons is especially important on small scales ($k > 1 \text{ Mpc}^{-1}$), which are also impacted by the relative motion effect.

3 FIRST HALOS AND THEIR GAS CONTENT

Both of the effects discussed above have a significant impact on the evolution of density perturbations on small scales and affect the formation of the first dark matter halos, as well as the subsequent accretion of the baryons and the formation of the first stars. We investigate the specific effects by studying the change in the characteristic mass scale that divides gas-rich and gas-poor halos produced by the relative velocity of the dark matter and baryonic fluids.

3.1 Filtering mass

In the Λ CDM universe, virialized dark matter halos form hierarchically on extremely small scales at very early times and start accreting baryons into their potential wells. If halos are heavy enough, accretion proceeds to the point where baryons start cooling through molecular line emission, condensing into the first stars and galaxies. This accretion is counteracted by the bulk motion of baryons with respect to dark matter as well as by the thermal gas pressure. The combination of the two effects leads to the presence of the minimal halo mass scale at which baryons are still able to effectively accrete onto a halo.

To study the effect of halo formation and baryonic accretion it is convenient to divide space into a large number of patches of the size of the relative velocity coherence scale. In each patch with a given mean density and bulk velocity, we follow the evolution of density perturbations including the spatial variation of the baryonic speed of sound due to Compton heating from the CMB (Naoz & Barkana 2005).

By evolving the system of equations (5) with the correct sound speed term of Eq. (7) in each patch, we calculate the baryonic and dark matter power spectra. Their ratio is constant on large scales (small k), and drops at high k due to the suppression of growth by the baryonic pressure. Gnedin & Hui (1998) originally defined a ‘‘filtering’’ scale (essentially a time-averaged Jeans scale) that they used to identify the largest scale on which the baryon fluctuations are substantially suppressed compared to those of the dark matter. We use the generalized definition from Naoz & Barkana (2007), in which the baryon-to-total ratio is expanded to linear order in k^2 , and written in the following form:

$$\frac{\delta_b}{\delta_{\text{tot}}} = 1 - \frac{k^2}{k_F^2} + r_{\text{LSS}},\quad (11)$$

where the total density perturbation $\delta_{\text{tot}} = f_b \delta_b + f_{\text{dm}} \delta_{\text{dm}}$

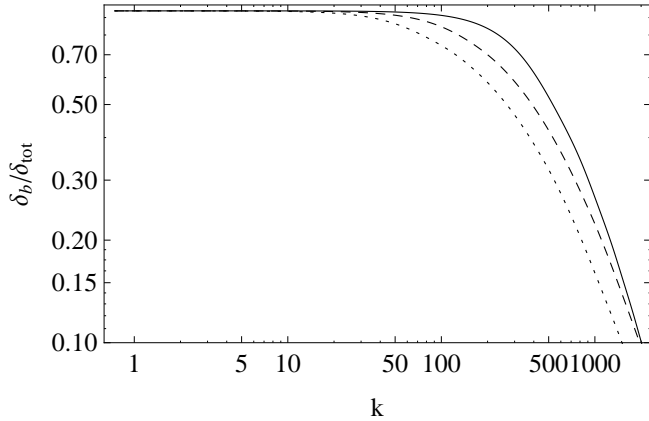


Figure 1. Perturbation ratio $\delta_b/\delta_{\text{tot}}$ vs. comoving wavenumber k evaluated at $z = 20$ for the cases of $v_{\text{bc}} = 0$ (solid curve), $v_{\text{bc}} = 1\sigma_{vbc}$ (dashed curve), and $v_{\text{bc}} = 2\sigma_{vbc}$ (dotted curve). In all cases overdensities are isotropically averaged over the direction of \mathbf{k} with respect to \mathbf{v}_{bc} .

(in terms of the cosmic baryon and dark matter mass fractions f_b and f_{dm}), and the k -independent r_{LSS} term (which is negative) describes the relative baryon-to-total difference in the limit of large scale structure, i.e., where both the v_{bc} effect and the thermal pressure of the gas are negligible (and restricted also to scales below the baryon acoustic oscillations).

In Fig. 1 we plot the isotropically averaged perturbation ratio $\delta_b/\delta_{\text{tot}}$ by averaging over the direction of \mathbf{k} with respect to \mathbf{v}_{bc} . On large scales the ratio is very close to constant, and using Eq. (11) we can deduce $r_{\text{LSS}} = -0.054$ at $z = 20$. The filtering scale k_F is obtained by fitting Eq. (11) to the calculated values of the ratio $\delta_b/\delta_{\text{tot}}$ from Fig. 1. This allows us to define the filtering mass in terms of the filtering wavenumber:

$$M_F = \frac{4\pi}{3}\bar{\rho}_0 \left(\frac{\pi}{k_F}\right)^3, \quad (12)$$

where $\bar{\rho}_0$ is the mean matter density today. We note that this relation is $\frac{1}{8}$ of the definition originally used by Gnedin (2000), who also used a non-standard definition of the Jeans mass.

The filtering mass plays an extremely important role in understanding the evolution of the first halos, as it provides a good approximation for the boundary between the gas-rich halos and halos that do not contain substantial quantities of gas. Traditionally one would assume that the separation between gas-rich and gas-poor objects is represented by the Jeans scale, which is the minimum scale on which a small gas perturbations will grow due to gravity overcoming the pressure gradient. However, the Jeans scale is related only to the evolution of the perturbations at a given point in time and does not account for significant variation of the Jeans mass with time. The filtering mass on the other hand reflects the baryonic pressure effects integrated over the entire history of the Universe, and provides a much better approximation to the boundary between gas-rich and gas-poor halos.

An extensive study of the filtering mass properties and evolution history in models without the relative ve-

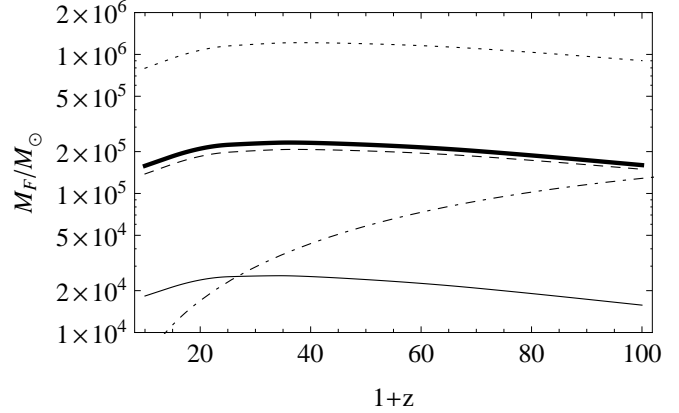


Figure 2. Evolution of the filtering mass with redshift in the regions with $v_{\text{bc}} = 0$ (thin solid line), $v_{\text{bc}} = 1\sigma_{vbc}$ (dashed line), $v_{\text{bc}} = 2\sigma_{vbc}$ (dotted line) and global average case (thick solid line). We also show the evolution of the Jeans mass M_J (dot-dashed line).

locity effect was performed in Naoz & Barkana (2005) and Naoz & Barkana (2007). The properties of the filtering mass, however, are significantly modified in the regions where the bulk motion of baryons with respect to dark matter potential wells is significant. In regions with high values of v_{bc} baryons tend to advect out of the collapsing dark matter halos, significantly increasing the filtering mass. We demonstrate this in Fig. 2 where we plot the evolution of the filtering mass with redshift in the regions with $v_{\text{bc}}/\sigma_{vbc} = 0, 1,$ and 2 . We also show the globally averaged case by integrating the filtering mass over the full probability distribution of the relative velocity, given by:³

$$P_{vbc}(v) = \left(\frac{3}{2\pi\sigma_{vbc}^2}\right)^{3/2} 4\pi v^2 \exp\left(-\frac{3v^2}{2\sigma_{vbc}^2}\right). \quad (13)$$

As noted earlier, the variance per axis is $\sigma_{vbc}^2/3$.

In Fig. 2 we also compare the filtering mass with the Jeans mass defined as:

$$M_J = \frac{4\pi}{3}\bar{\rho}_0 \left(\frac{\pi}{k_J}\right)^3, \quad (14)$$

where $k_J = \sqrt{2/3}aH/c_s$ is the Jeans scale (defined by setting the right-hand side of Eq. (5) to zero, without the relative velocity term, and neglecting here the correction of Eq. (7)). Fig. 2 shows that the filtering mass reaches a maximum value at redshift $z \sim 40$ (and generally varies only slightly throughout the plotted redshift range), whereas the Jeans mass continuously decreases with time due to the drop in the sound speed of the gas as the Universe cools.

The filtering mass represents a time averaged Jeans mass and hence it decreases at the low redshifts, however, right after recombination baryonic perturbations on small

³ This is the distribution of the magnitude of v_{bc} , where the vector \mathbf{v}_{bc} is the result of linear perturbations and hence is drawn from a multivariate Gaussian. It thus happens to be the same as the Maxwell-Boltzmann distribution, even though the bulk velocities of baryons have nothing to do with thermal motions of particles.

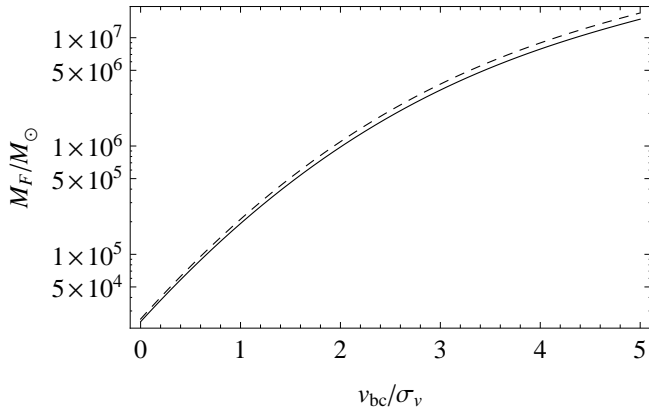


Figure 3. This figure shows the filtering mass M_F as a function of the relative velocity of the dark matter and baryonic fluids at $z = 20$ (solid line) and $z = 40$ (dashed line).

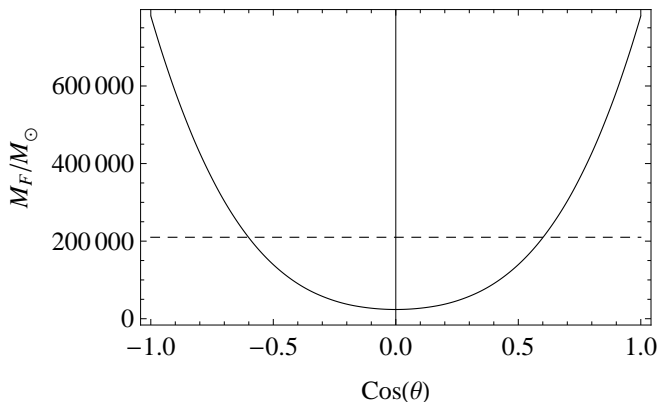


Figure 4. The lower panel shows the dependence of the filtering mass on the angle θ between the directions of \mathbf{v}_{bc} and the wavevector \mathbf{k} (solid line), and the isotropically averaged value of M_F (dashed horizontal line), in regions where $v_{bc} = 2\sigma_{vbc}$ at $z = 20$.

scales are highly suppressed and they only catch up gradually, causing the filtering mass to increase from low initial values. We emphasize that in the regions with a high value of the relative velocity the filtering mass is significantly larger than in the regions with small values of v_{bc} and hence the formation of gas-rich objects in those regions proceeds quite differently than in the regions with $v_{bc} \sim 0$. The filtering scale and mass (from Eqs. (11) and (12)) in regions with varying values of v_{bc} are given in Table 1, and the filtering masses at $z = 20$ and $z = 40$ are plotted in Fig. 3. In Fig. 4, we also show the dependence of the filtering mass on the angle θ between the direction of \mathbf{v}_{bc} and that of the wavevector \mathbf{k} in regions where $v_{bc} = 2\sigma_{vbc}$ at $z = 20$; the plot shows that the main contribution to the filtering mass comes from the regions where the wavenumber \mathbf{k} and the relative velocity vector \mathbf{v}_{bc} are parallel (or anti-parallel).

3.2 Gas content of the first galaxies and minihalos

We now investigate the amount of gas that falls into early haloes, and how much of this gas is capable of cooling. Here we use analytical approximations – namely the relation be-

v_{bc}/σ_{vbc}	$P(> v_{bc})$	k_F (Mpc $^{-1}$)	M_F (M_\odot)
4	2.1×10^{-10}	85	7.75×10^6
3	5.9×10^{-6}	113	3.37×10^6
2	7.4×10^{-3}	166	1.07×10^6
1	0.392	298	1.85×10^5
0	1	591	2.39×10^4

Table 1. Filtering scale and filtering mass for the isotropic averaging of the direction of \mathbf{k} with respect to \mathbf{v}_{bc} at $z = 20$.

tween the gas mass fraction f_g and filtering mass M_F , and the Sheth & Tormen (1999) mass function – that have been calibrated against simulations with statistically isotropic initial conditions and no bulk relative velocity. In our case with $v_{bc} \neq 0$ the power spectra are both reduced and slightly anisotropic, but we expect these approximations to still be a useful guide since statistical anisotropy (e.g. θ -dependent filtering mass) can only appear at second order in scalars such as the halo mass function or gas content.

There is no *a priori* reason to suppose that the filtering mass, which is defined based on linear perturbations, can also accurately describe properties of highly nonlinear, virialized objects. Qualitatively we may argue that if pressure significantly opposes gravity during the halo formation process (which for some time is accurately described by linear theory) then it will significantly suppress the amount of gas in the final virialized halo. Gnedin (2000) suggested based on simulations during cosmic reionization that the filtering mass accurately fits the mass for which a halo contains half the mean cosmic baryon fraction f_b , and fitted the simulation results to the following formula:

$$f_g = f_{b,0} \left[1 + \left(2^{\alpha/3} - 1 \right) \left(\frac{M_F}{M} \right)^\alpha \right]^{-3/\alpha}, \quad (15)$$

where $f_{b,0}$ is the gas fraction in the high-mass limit. In this function, a higher α causes a sharper transition between the high-mass (constant f_g) limit and the low-mass limit (assumed to be $f_g \propto M^3$). This formula has subsequently been found to agree with hydrodynamic simulations (Naoz, Barkana & Mesinger 2009; Naoz, Yoshida, & Barkana 2010) if we set $\alpha \approx 0.7$ and $f_{b,0} = f_b(1 + 3.2r_{LSS})$ (Barkana & Loeb 2010), and use the filtering mass as defined in Eq. (12) (which differs from Gnedin (2000), as noted earlier). Thus, at each redshift, in each patch of the Universe we may calculate the local value of M_F and from it the gas fraction in halos of various total mass. In Fig. 5, we plot the gas fraction as a function of halo mass in regions with varying values of relative velocity at $z = 20$. It is clear that halos that would be gas-rich in the Universe with no v_{bc} effect become gas-poor in the regions where the relative velocity is high. We also see that on average, introduction of the v_{bc} effect significantly lowers the gas fraction in all halos with $M_h < 10^7 M_\odot$.

In order to find the total amount of gas in galaxies, we must integrate over the halo mass function in each patch. We start with the $v_{bc} = 0$ case. Standard models for halo formation are based on spherical collapse calculations, in which the linear overdensity must reach a critical threshold $\delta_c(z)$ for the corresponding region to form a collapsed halo at redshift z . The halo abundance depends on the statistics of fluctuations on various scales, which can be parameterized

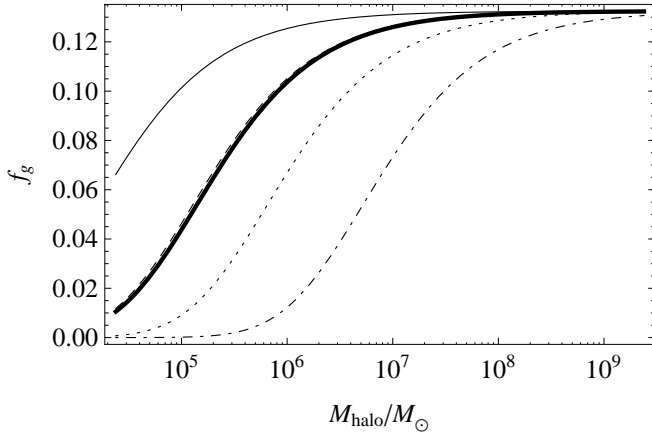


Figure 5. Change in the gas fraction f_g at $z = 20$ as a function of halo mass for regions with $v_{bc} = 0$ (thin solid line), $v_{bc} = 1\sigma_{vbc}$ (dashed line), $v_{bc} = 2\sigma_{vbc}$ (dotted line), $v_{bc} = 4\sigma_{vbc}$ (dash-dotted line) and isotropically averaged case (thick solid line, nearly coincident with the dashed line).

by the function $S(R)$, the variance of fluctuations in spheres of radius R (S is also a function of redshift). In general we define $f(\delta_c(z), S) dS$ to be the mass fraction contained at z within halos with mass in the range corresponding to S to $S + dS$. We convert between halo mass M and (initial comoving) radius R using the cosmic mean density. The halo abundance is then

$$\frac{dn}{dM} = \frac{\bar{\rho}_0}{M} \left| \frac{dS}{dM} \right| f(\delta_c(z), S), \quad (16)$$

where dn is the comoving number density of halos with masses in the range M to $M + dM$. In the model of Press & Schechter (1974),

$$f_{\text{PS}}(\delta_c(z), S) = \frac{1}{\sqrt{2\pi}} \frac{\nu}{S} e^{-\nu^2/2}, \quad (17)$$

where $\nu = \delta_c(z)/\sqrt{S}$ is the number of standard deviations that the critical collapse overdensity represents on the mass scale M corresponding to the variance S .

However, the Press-Schechter mass function fits numerical simulations only qualitatively, and in particular it substantially underestimates the abundance of the rare halos that host galaxies at high redshift. The halo mass function of Sheth & Tormen (1999), which fits numerical simulations much more accurately, is given by

$$f_{\text{ST}}(\delta_c(z), S) = A' \frac{\nu}{S} \sqrt{\frac{a'}{2\pi}} \left[1 + \frac{1}{(a'\nu^2)^{q'}} \right] e^{-a'\nu^2/2}, \quad (18)$$

with best-fit parameters (Sheth & Tormen 2002) $a' = 0.75$ and $q' = 0.3$, and where the normalization to unity is ensured by taking $A' = 0.322$.

The critical density of collapse $\delta_c(z)$ is independent of mass and equals 1.69 in the Einstein de-Sitter limit, valid over a wide range of redshifts. Its value decreases at low redshift due to the cosmological constant, but more relevant for this paper is the decrease at very high redshift due to the effects of the baryons and radiation. The decrease is by $\sim 0.05(1+z)$ per cent from the Einstein de-Sitter value (Naoz & Barkana 2007), a small effect that is however

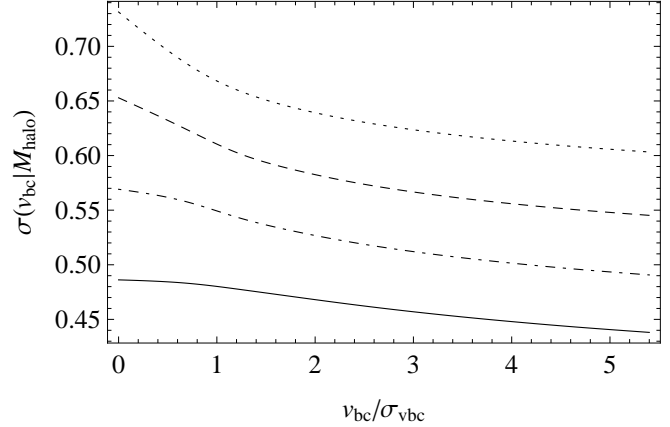


Figure 6. Dependence of $\sigma(v_{bc}|M_h)$ on the relative velocity v_{bc} at $z = 20$ for a fixed mass of the collapsed halos: $M_h = 10^7 M_\odot$ (solid line), $M_h = 10^6 M_\odot$ (dot-dashed line), $M_h = 10^5 M_\odot$ (dashed line), and $M_h = 10^4 M_\odot$ (dotted line).

greatly amplified by the fact that galaxies at the highest redshifts form in halos that correspond to very rare density fluctuations.

In our approach we must calculate how the halo mass function varies in different regions. The Press-Schechter model has been extended (Bond et al. 1991) to describe the variation of the halo abundance in regions of various density, and we can generalize this to include the bulk velocity by including the variation of the function $S(R)$ with v_{bc} . To demonstrate this dependence we plot in Fig. 6 $\sqrt{S} \equiv \sigma(v_{bc}|M_h)$ as a function of the relative velocity at a fixed halo mass M_h . We see that the variance of the density perturbations decreases with increasing v_{bc} , leading to a delay in the collapse of dark matter halos. We also find that the change in σ is larger for halos of low mass since the power spectrum on scales much larger than the filtering mass is unaffected by the relative velocity.

We can summarize the important effects of the change in halo abundance and halo gas content at a given mass scale by calculating various gas fractions at each redshift. This can be done by using the Sheth-Tormen mass function and accounting for the changes due to the relative velocity effect. We calculate the fraction of the total matter density in halos above a certain mass scale by

$$f_{\text{tot}}(> M_h) = \int_{M_h}^{\infty} \frac{M}{\bar{\rho}_0} \frac{dn}{dM} dM, \quad (19)$$

and the fraction of the baryon density contained in those halos using Eq. (15):

$$f_{\text{gas}}(> M_h) = \int_{M_h}^{\infty} \frac{M}{\bar{\rho}_0} \frac{dn}{dM} \frac{f_g}{f_b} dM. \quad (20)$$

We plot both fractions in Fig. 7 at $z = 20$ for $v_{bc}/\sigma_{vbc} = 0, 1, \text{ and } 2$, and for the globally averaged case, where we take into consideration the global distribution of the v_{bc} . The plot clearly shows that in regions with high relative velocity the gas fraction in halos is dramatically suppressed. The global average (which comes out very close to the $v_{bc}/\sigma_{vbc} = 1$ case) gives a suppression by a factor of 2.7 of the total gas fraction in halos. In order to separate out the various effects, we plot one case in which we use the correct halo

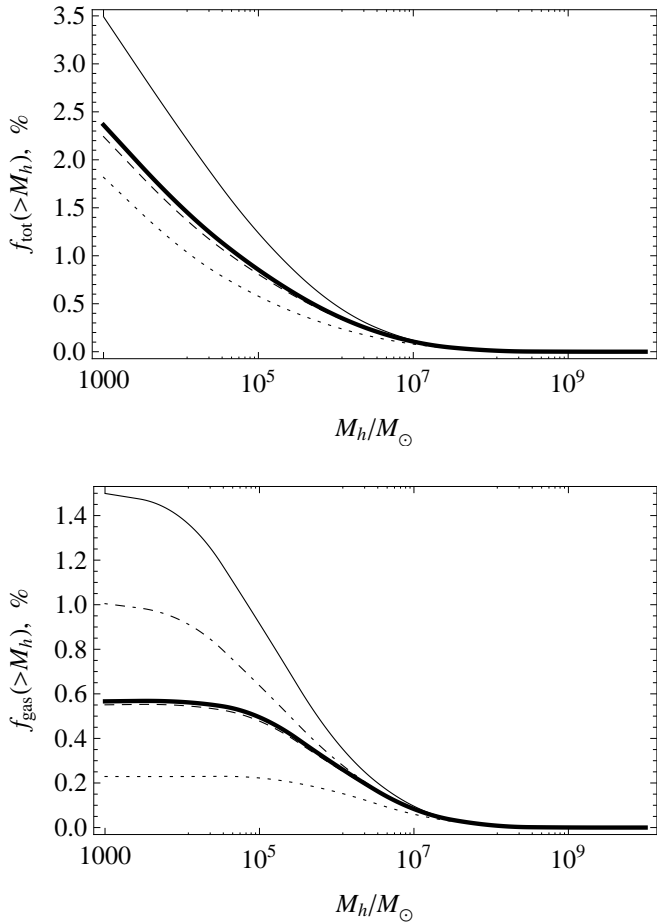


Figure 7. The mass fraction in halos above M_h (upper panel) and the gas fraction in halos (lower panel) at redshift $z = 20$ for the case $v_{bc}/\sigma_{vbc} = 0$ (thin solid line), 1 (dashed line), 2 (dotted line), and for the globally averaged case (thick solid line). In the lower panel we also show the case where we fix the value of M_F as calculated for $v_{bc} = 0$ and use the correct globally averaged halo mass function including the variation with v_{bc} (dot-dashed line).

mass function (as it varies with v_{bc}) but fix the filtering mass to the $v_{bc} = 0$ value. We find that the suppression arises from comparable contributions from the change in halo numbers (about a factor of 1.8) and from the reduction in the internal halo gas fractions (about a factor of 1.5).

Stars are understood to form at high redshift out of gas that cooled and subsequently condensed to high densities in the cores of dark matter halos. Since metals are absent in the pre-stellar universe, the earliest available coolant is molecular hydrogen (H_2), and thus the minimum halo mass that can form a star is set by requiring the infalling gas to reach a temperature of several hundred Kelvin required for exciting H_2 to the $J \geq 2$ rotational levels (Tegmark et al. 1997). This has been confirmed with high-resolution numerical simulations containing gravity, hydrodynamics, and chemical processes in the primordial gas (Abel, Bryan & Norman 2002; Bromm, Coppie & Larson 2002; Fuller & Couchman 2000; Yoshida et al. 2003; Reed et al. 2005). These simulations imply a minimum halo circular velocity $V_c \sim 4.5 \text{ km s}^{-1}$ for forming a star, where $V_c = \sqrt{GM/R}$ in terms of the halo

virial radius R . The simulations show that in a halo above the minimum mass (which at $z = 20$ is $M_{\min} \approx 6 \times 10^5 M_\odot$), the gas cools in the dense center and forms at least one star very quickly; this is understood theoretically since both the cooling time and the dynamical time are a small fraction of the cosmic age at that time. We are thus interested in the total gas fraction in halos above this cooling threshold; if there is a fixed star formation efficiency in these halos, then the this gas fraction is directly proportional to the stellar density in each region.

We plot in Fig. 8 the evolution of various gas and total mass fractions as a function of redshift. Even without the relative velocity effect, there is some (spatially-uniform) suppression predicted for the gas fraction in halos that can cool (i.e., a suppression of the overall star formation) by a factor of 1.2 at $z = 20$ and 1.5 at $z = 40$ (relative to the cosmic baryon fraction); this is due to the fact that the baryon perturbations are still catching up to the dark matter perturbations at these redshifts, even on large scales (beyond the filtering mass), and simulations suggest that non-linear halo formation amplifies the remaining differences (Naoz, Yoshida, & Barkana 2010; Barkana & Loeb 2010). The relative velocity effect adds an additional suppression of cosmic star formation by a factor of 1.6 at $z = 20$ and 3.4 at $z = 40$. The relative velocities have a larger effect on the gas in minihalos, the smaller halos that accrete gas that cannot cool. Since the total mass fraction in halos continues to increase as we consider smaller and smaller halo masses (Fig. 7), the total amount of gas in minihalos is very sensitive to the filtering mass, which is what produces the (gradual) low-mass cutoff in gas accretion onto halos. In the absence of the relative velocities, the total gas fraction in halos at $z = 20$ is 1.5×10^{-2} , consisting of 1.0×10^{-2} in minihalos and 5×10^{-3} in galaxies. At $z = 40$, these gas fractions are 2.4×10^{-5} , 2.3×10^{-5} , and 1×10^{-6} , respectively. The relative velocities, in the global average, reduce these fractions to 6×10^{-3} , 3×10^{-3} , and 3×10^{-3} at $z = 20$, and 1.5×10^{-6} , 1.1×10^{-6} , and 4×10^{-7} at $z = 40$. Note that the gas fraction above the H_2 cooling mass is really an upper limit to the gas fraction that undergoes star formation. Any significant feedback effect will raise the effective threshold for star formation, making the total gas fraction in halos correspond almost completely to star-less halos (see discussion in Sec. 4).

3.3 Probability distribution functions

In addition to plotting mean values of various quantities, it is interesting to consider their variation in various regions. Above, we have explicitly varied v_{bc} but averaged over the density fluctuations (note that the density and velocity are uncorrelated at a given point). However, in order to calculate the full amount of variation of various quantities, i.e., the probability distribution function (PDF), we must explicitly vary both the mean density and the value of v_{bc} in each region.

In the absence of relative velocities, the extended Press-Schechter model gives the variation of the Press-Schechter halo mass function in regions of various mean density. No analytical generalization of this formalism is known for the more accurate Sheth-Tormen model, but Barkana & Loeb (2004) suggested a hybrid prescription that adjusts the

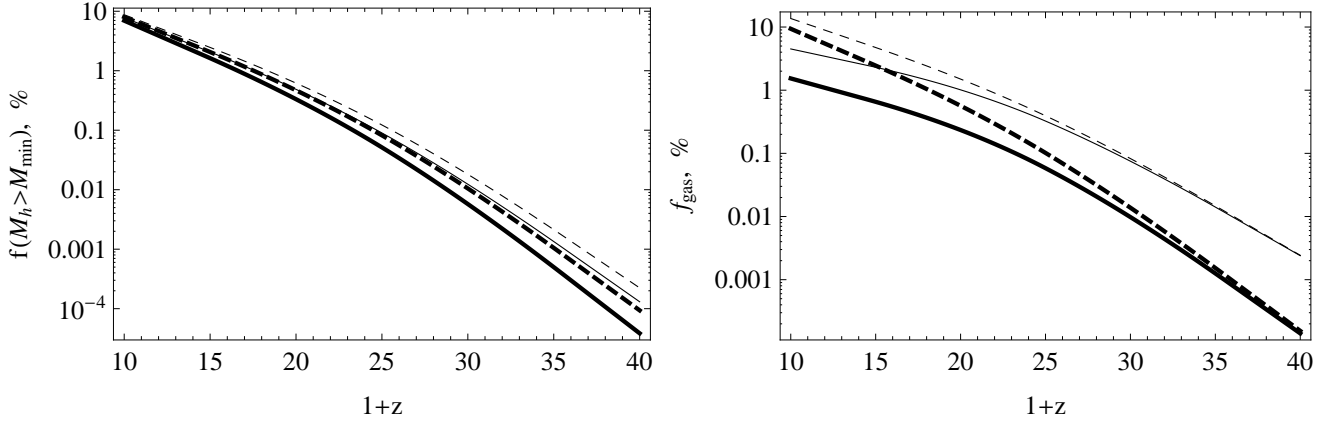


Figure 8. In the left panel we plot the total mass fraction in halos above the cooling mass (dashed lines) and total gas fraction in halos above the minimum cooling mass (solid lines). In the right panel we show total gas fraction in halos (dashed lines) and gas fraction in minihalos, i.e., in halos below minimum cooling mass (solid lines). All plots show two cases: no v_{bc} (regular lines) and the correct case where the v_{bc} effect is taken into account and the isotropic averaging is performed (thick lines).

abundance in various regions based on the extended Press-Schechter formula, and showed that it fits a broad range of simulation results. Generalizing this prescription to include the effect of relative velocity, we set

$$f_{\text{bias}}(\delta_c(z), \bar{\delta}_R, R, M, v_{bc}) = \left[\frac{f_{\text{ST}}(\delta_c(z), S')}{f_{\text{PS}}(\delta_c(z), S')} \right] \times f_{\text{PS}}(\delta_c(z) - \bar{\delta}_R, S' - S'(R)), \quad (21)$$

where the mean overdensity in the patch is $\bar{\delta}_R$, and for a given halo mass, the variance S' is calculated using the power spectrum modified by the local bulk velocity. The subtraction of $S'(R)$ accounts for the fact that $\bar{\delta}_R$ arises from density modes on scales larger than the patch size, leaving only the remaining variance $S' - S'(R)$ for fluctuation modes within the patch to supply the additional density needed to reach $\delta_c(z)$ and thus form a halo. In our case, the patches in which we will compute the baryon collapse fraction PDF will be spheres of radius $R = 3$ Mpc (comoving). Note that if used to compute a mass function, the above formula gives the Lagrangian halo number density, while the Eulerian density is larger by a factor of $1 + \bar{\delta}_R$; however no such transformation is necessary to compute the local *fraction* of gas in halos.

We start by calculating the PDF for the filtering mass M_F . In the scenario without v_{bc} we would have a universal value of M_F , however, since various regions of space have different values of relative velocity of baryonic and dark matter fluids this produces a variation in M_F . The distribution of relative velocities is given by Eq. (13) and it translates into the distribution of M_F using:

$$P_{M_F}(M_F) = P_{v_{bc}}(v_{bc}) \frac{dv_{bc}}{dM_F}. \quad (22)$$

The PDF of the filtering mass at $z = 20$ and $z = 40$ is plotted in Fig. 9. These distribution functions are essentially determined by the distribution of the relative velocity and exhibit clear peaks which correspond to values of the filtering mass around the maximum of the v_{bc} distribution, which occurs at $v_{bc} \approx 1.2\sigma_{v_{bc}}$. As noted before (Figs. 2 and 3), the filtering mass does not vary much in this redshift range, but

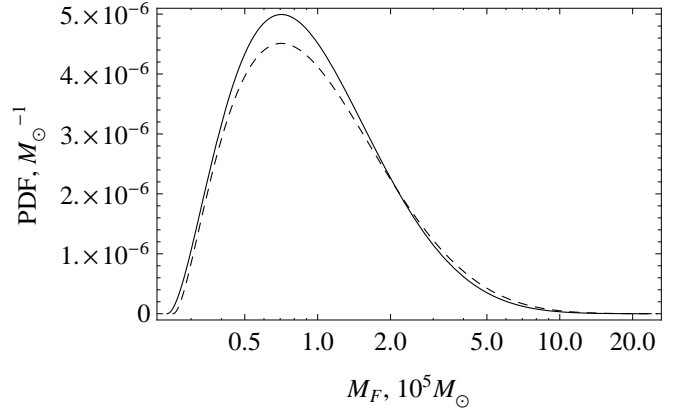


Figure 9. The PDF of the filtering mass M_F at $z = 20$ (solid line) and $z = 40$ (dashed line). We consider cells of radius $R = 3$ Mpc, and include the variation of v_{bc} as well as the mean density in each cell.

at $z = 20$ it is slightly more sharply peaked while the PDF at $z = 40$ extends more towards high values of M_F . Filtering mass has a rather significant scatter with the full width at half maximum $\sim 1.5 \times 10^5 M_\odot$ at the redshift of $z = 20$.

To better understand global properties of the first objects we calculate probability distribution functions of the total gas fraction in halos as well as the gas fraction in halos above the minimum cooling mass M_{min} . As noted earlier, these gas fractions are affected by the distribution of relative velocities as well as the distribution of large scale overdensities $\bar{\delta}_R$. We consider the PDF of gas fractions inside spherical regions (“cells”) of radius $R = 3$ Mpc, which are small enough that v_{bc} can be treated as roughly constant over a cell. We obtain the PDFs by running a Monte Carlo simulation that generates random values of v_{bc} using Eq. (13) and of the large-scale overdensity within the cell $\bar{\delta}_R$ using a Gaussian of variance $S'(R)$. In Fig. 10 we show the PDFs of the gas fractions in halos above and below the minimum cooling mass $M_{\text{min}} \approx 6 \times 10^5 M_\odot$ at $z = 20$. We also show the same distributions for the case with no v_{bc} effect. The figure

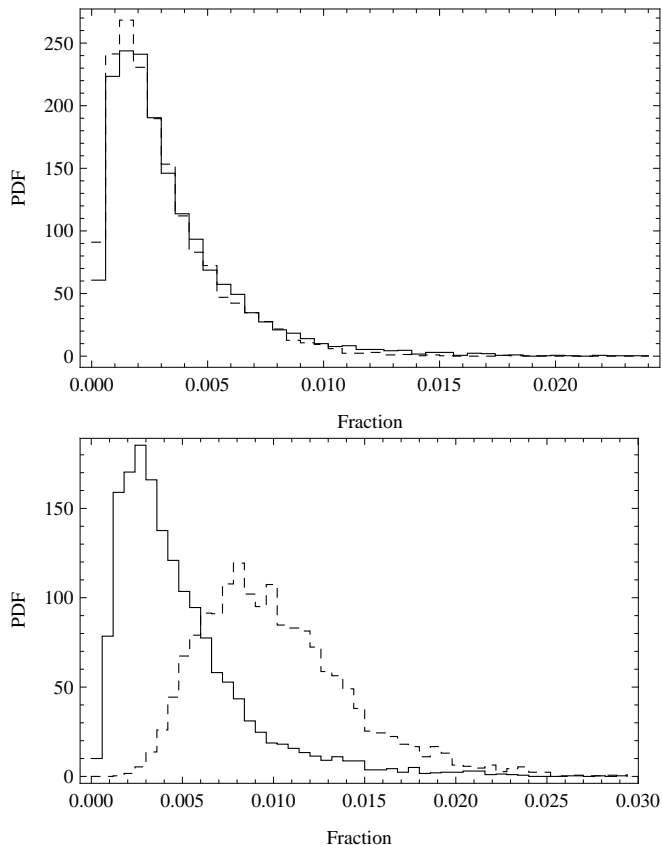


Figure 10. The PDFs of the gas fraction in halos above the minimum cooling mass (solid line), and the gas fraction in minihalos, i.e., halos below the minimum cooling mass (dashed line) at $z = 20$ for the case with the v_{bc} effect (upper panel) and without the effect (lower panel).

shows how minihalos would be dominant at $z = 20$ (by a factor of 2 compared to galaxies), but since v_{bc} has a larger effect on the minihalos, it makes the gas content roughly equal between galaxies and minihalos at this redshift. Each PDF has a non-Gaussian extension towards high fractions (in fact, the distribution is approximately lognormal). Thus, the peak of the PDF is significantly lower than the mean value; without the relative velocity it is 0.002 for galaxies and 0.008 for minihalos, and v_{bc} moves it to ~ 0.0015 for both. Also, the relative velocities reduce the full width at half maximum from 0.004 (galaxies) and 0.008 (minihalos) to 0.003 for both.

4 CONCLUSIONS

We have shown that the relative velocity of baryons and dark matter has a significant impact on the properties of the first bound objects and has to be considered in detailed studies of the epoch of reionization and especially earlier epochs. The supersonic motion of the baryonic fluid relative to the underlying potential wells created by the dark matter causes advection of small-scale perturbations by large-scale velocity flows, leading to a significant suppression of gas accretion during halo formation and dramatically increasing the characteristic mass of gas-rich objects at high redshifts

($z > 10$). In particular, instead of this characteristic filtering mass being close to the Jeans mass of $2 \times 10^4 M_\odot$ at $z = 20$, it varies among various regions from this value up to $\sim 10^6 M_\odot$, with a 1σ value (and global average) around $M_F = 2 \times 10^5 M_\odot$, i.e., an order of magnitude higher than without the relative velocity effect.

The relative velocity effect also modifies the star formation history, delaying star formation and causing significant spatial fluctuations. However, since the minimum mass for H_2 cooling ($\approx 6 \times 10^5 M_\odot$ at $z = 20$) is somewhat higher than the average M_F , the suppression effect of v_{bc} is limited to about a factor of 1.6 at $z = 20$ (added on top of the spatially-uniform factor of 1.2 from the still-depressed baryon perturbations on large scales), compared to a much larger effect (a factor of 3.3) on the gas fraction in star-less gas minihalos. The importance of the relative velocity grows steadily with redshift, so that at $z = 40$ the suppression factors due to v_{bc} increase to 2.5 for galaxies (on top of a pre-existing factor of 1.5) and 21 for minihalos.

In our detailed treatment, we included the spatial variation of the baryonic sound speed, the suppression of baryonic perturbations on large scales, and the effect of the relative velocity, through the modified power spectrum, both on the halo mass function and the internal gas fractions in halos. In order to gauge the induced spatial variability, we further calculated the full probability distribution functions of the characteristic mass and of gas fractions inside of the first collapsed halos. These results are important for understanding of the relative velocity effect on large scales, and we plan to study them further.

Our results significantly extend the work done recently by Dalal, Pen & Seljak (2010). For example, we find a suppression factor due to v_{bc} at $z = 20$ of 1.6 and 3.3, for star-forming halos and minihalos, respectively. In their approach Dalal, Pen & Seljak (2010) did not separate these two categories, and found a factor of 2.5 suppression in the collapsed fraction, which under their approximation can be interpreted as a suppression of star formation. In our work we removed this and many other approximations used in Dalal, Pen & Seljak (2010). Comparing to our work, we expect that their calculation of Lyman- α flux fluctuations is qualitatively correct but may be somewhat overestimated and requires a more detailed analysis.

As we were finishing this paper, two simulation papers appeared on the effect of v_{bc} at high redshift (Maio et al. 2010; Stacy et al. 2010). While both found a small suppression of star formation, their results appear at first glance to show a smaller suppression effect than we predict. This difference is not surprising if we note that these simulation papers focused on star-forming halos around $z \approx 15$, while the largest effects that we find occur for star-less minihalos at higher redshifts. At $z > 20$, Maio et al. (2010) find tens of percents difference in the gas fractions, although the statistical errors are large. Stacy et al. (2010) find a delay in gas collapse by $\Delta a/a = 0.14$ for $v_{bc}/\sigma_{vbc} = 1$. We also note that the choice of initial conditions should be carefully considered: standard initial condition codes do not properly treat the separate baryonic and dark matter perturbations or the gas temperature perturbations, leading to a filtering mass that is too high by a factor of ~ 2 at $v_{bc} = 0$ (Naoz, Yoshida, & Barkana 2010); as such they may underestimate the effect of relative velocities.

The simulations by Maio et al. (2010) and Stacy et al. (2010) clearly represent a very important step and will serve as a good foundation for simulations with larger boxes and improved initial conditions. Eventually we hope that simulations including v_{bc} will advance to the point where improved fitting functions for the local halo mass function and gas mass fraction become available.

We note that various feedback effects may reduce or mask some of the effect of the relative velocity. For galaxies, local feedback from star formation may effectively raise the minimum halo mass for star formation (except for the very first generation of stars). The possibilities include supernova feedback as well as radiative feedback acting via photoheating and photoevaporation or suppression of H_2 formation, although “positive” feedback due to X-ray ionization enhancing H_2 formation has also been suggested (Haiman et al. 1996, 1997). For minihalos, astrophysical heating, e.g., from an early X-ray background, may heat the gas and raise the filtering mass above the value due to v_{bc} . There are many unknowns, but these various effects could begin to be significant by $z \sim 20$, and very likely by the time of significant cosmic reionization. Still, the relative velocity between baryons and dark matter is the main determinant of the gas content of halos at the highest redshifts.

ACKNOWLEDGMENTS

D.T. and C.H. are supported by the U.S. Department of Energy (DE-FG03-92-ER40701) and the National Science Foundation (AST-0807337). C.H. is supported by the David and Lucile Packard Foundation. R.B. is supported by Israel Science Foundation grant 823/09.

REFERENCES

- Abel, T. L., Bryan, G. L., & Norman, M. L. 2002, *Science* 295, 93
- Barkana R., Loeb A., 2001, *Phys.Rept.* 349, 125
- Barkana R., Loeb A., 2004, *ApJ*, 609, 474
- Barkana R., Loeb A., 2002, *ApJ*, 578, 1
- Barkana R., Loeb A., 2005, *ApJ*, 626, 1
- Barkana, R., Loeb, A., 2010, *MNRAS*, submitted (arXiv1009.1393)
- Bennett C. et al, 2003, *ApJS*, 148, 1
- Bond J. R., Cole S., Efstathiou G., Kaiser N., 1991, *ApJ*, 379, 440
- Bromm V., Coppie P. S., Larson R. B., 2002, *ApJ*, 564, 23
- Ciardi B., Scannapieco E., Stoehr F., Ferrara A., Iliev I., Shapiro P., 2005, *MNRAS*, 366, 689
- Dalal, N., Pen, U.L., Seljak, U., 2010, *JCAP*, 11, 007
- Eisenstein D., Hu W., 1998, *ApJ*, 496, 605
- Fuller, T. M., Couchman, H. M. P., 2000, *ApJ*, 544, 6
- Furlanetto S., Oh S. P., 2006, *ApJ*, 652, 849
- Gnedin N. Y., 2000, *ApJ*, 542, 535.
- Gnedin N. Y., Hui L., 1998, *MNRAS*, 296, 44.
- Haiman Z., Abel T., Madau P., 2001, *ApJ*, 551, 599
- Haiman, Z., Rees, M. J., & Loeb, A. 1996, *ApJ*, 467, 522
- Haiman, Z., Rees, M. J., & Loeb, A. 1997, *ApJ*, 476, 458; erratum, 484, 985
- Iliev I., Scannapieco E., Martel H., Shapiro P., 2003, *MNRAS*, 341, 81
- Iliev I., Scannapieco E., Shapiro P., 2005, *ApJ*, 624, 491
- Komatsu, E., et al., 2010, *ApJS*, submitted (arXiv1001.4538)
- Lewis A., Challinor A., 2007, *PRD*, 76, 083005
- Madau P., Meiksin A., Rees M., 1997, *ApJ*, 475, 429
- Maio, U., Koopmans, L. V. E., & Ciardi, B. 2010, arXiv:1011.4006
- Naoz S., Barkana R., 2005, *MNRAS*, 362, 1047
- Naoz S., Barkana R., 2007, *MNRAS*, 377, 667
- Naoz S., Barkana R., Mesinger A., 2009, *MNRAS*, 377, 667
- Naoz S., Yoshida, N., Barkana R., 2010, *MNRAS*, submitted (arXiv1009.0945)
- O’Shea B., Abel T., Whalen D., Norman M., 2005, *ApJL*, 628, L5
- Press W. H., Schechter P. 1974, *ApJ*, 187, 425
- Reed D. S. et al. 2005, *MNRAS*, 363, 393
- Sheth R. K., Tormen G., 1999, *MNRAS*, 308, 119
- Sheth R. K., Tormen G., 2002, *MNRAS*, 329, 61
- Stacy, A., Bromm, V., & Loeb, A. 2010, arXiv:1011.4512
- Tegmark M. et al., 1997, *ApJ*, 474, 1
- Tseliakhovich D., Hirata C. M., 2010, *PRD*, 82, 083520
- Yoshida N., Sokasian A., Hernquist L., Springel V., 2003, *ApJ*, 598, 73
- Yoshida N., Omukai K., Hernquist L., *Science*, 321, 669